The International Journal of Advanced Manufacturing Technology (2019) 103:311–324
https://doi.org/10.1007/s00170-019-03479-7

ORIGINAL ARTICLE

Effects of air on metallic sheet deformation by electromagnetic forming

Ning Liu [1,2] · Zhipeng Lai [1,2] · Quanliang Cao [1,2] · Xiaotao Han [1,2] · Yujie Huang [1,2] · Xiaoxiang Li [1,2] · Meng Chen [1,2] · Liang Li [1,2]

Received: 8 November 2018 / Accepted: 18 February 2019 / Published online: 19 March 2019

Abstract
Air is one of the most important processing parameters in electromagnetic sheet metal forming processes, especially when forming a large-scale sheet via single discharge or controlling dimensional accuracy with the die fitness of the deformed workpiece. Previous research on electromagnetic sheet forming mostly concentrated on the effects of magnetic pressure distribution, discharge energy, and material properties on workpiece deformation behavior. In this paper, the effect of air on electromagnetic sheet forming is investigated and the research contents are mainly divided into the following three parts: (1) investigating the influence of thickness, material strength, and die caliber on pre-deformation of the sheet when the die cavity is an approximate vacuum via simulation and experimentation; (2) studying the effect of workpiece pre-deformation on electromagnetic sheet forming with regard to the magnitude and distribution of the electromagnetic force, deformation velocity, workpiece profile, etc.; and (3) investigating the influence of the resistance generated by the residual die cavity air on workpiece deformation with experiments considering the die fitness of the deformed workpiece. The results show that atmospheric pressure results in workpiece pre-deformation when the die cavity is near vacuum and the pre-deformation is closely related to the workpiece thickness, material strength, and die caliber. The Lorentz force distribution moves toward the region near the chamfer of the die, and the peak value of the Lorentz force and the deformation velocity of the workpiece are reduced by 62% and 26.9%, respectively, when considering workpiece pre-deformation. The resistance caused by residual air will obviously affect workpiece deformation. The influence will weaken as air pressure decreases, and the maximum deviation of the workpiece formed by a single discharge is less than 1.5% when the air pressure is reduced to 30 Pa.

Keywords Air resistance · Electromagnetic sheet forming · Pre-deformation · Air pressure

1 Introduction

Energy savings and emission reduction are two of the most important concerns of the current manufacturing industry. Lightweight materials such as aluminum alloys are effective substitutes for traditional steel because of their lower density and higher intensity. However, aluminum alloys exhibit poor formability in traditional forming processes at room temperature, which limits their application to a certain extent. Fortunately, some scholars have found that a high-speed forming process can significantly improve the formability of aluminum alloys. As a high-speed forming method, electromagnetic forming (EMF) has been proven to have many advantages, such as springback reduction, wrinkling inhibition, and forming limit increase of materials [1]. Therefore, this technique has been extended to form various types of workpieces, including sheet metal [2], tubes [3, 4] and electromagnetics powder compaction [5].

In electromagnetic sheet metal forming, the distribution of magnetic pressure, which has been deeply investigated, influences workpiece deformation behavior. Takatsu et al. [6] found that the inhomogeneity of the radial distribution of magnetic pressure has a strong effect on the initial stage of sheet deformation in both numerical simulations and annealed aluminum sheet free bulging experiments using a flat spiral coil.

✉ Liang Li
liangli44@mail.hust.edu.cn

[1] Wuhan National High Magnetic Field Center, Huazhong University of Science and Technology, Wuhan 430074, China

[2] State Key Laboratory of Advanced Electromagnetic Engineering and Technology, Huazhong University of Science and Technology, Wuhan 430074, China

To provide a uniform electromagnetic force, Oliveira et al. [7] used a double spiral coil to avoid the "dead spot" at the spiral coil center. Kamal and Daehn [8] proposed a new coil structure that provides a much more uniform electromagnetic pressure and higher efficiency in forming sheet metal. Ahmed et al. [9] demonstrated a flat spiral coil conceptual design to modify the distribution of electromagnetic force by defining the pitch and cross-sectional area of the conductor increase from the center to the outer turn along a radial axis. For electromagnetic sheet metal forming, the interaction between workpiece deformation and the distribution of electromagnetic force also plays an important role. Kleiner et al. [10] showed that the pressure impulse is short compared to the workpiece deformation duration, especially for sheet metal forming, thus indicating that inertia had a significant influence on sheet deformation.

In addition, many efforts have focused on applications of new processing methods and the roles of process parameters in electromagnetic sheet forming. Shang and Daehn [11] formed a non-symmetric metal panel of Al 6111-T4 by applying electromagnetically assisted stamping (EMAS); the draw depth was increased by 44% compared to conventional stamping. Cui et al. [12] proposed combining electromagnetic incremental forming with stretching forming and manufactured a large part after discharging 36 times and stretching 6 times. Lai et al. [13, 14] developed a novel dual-coil system to provide an extra radial Lorentz force in deep drawing experiments and increased the forming depth of a cup-shaped part by 140%. Cui et al. [15] tried to find the optimum current frequency in terms of sheet thickness and current damping exponent and found that the optimum frequency is closely related to the thickness and current damping exponent for a given discharge voltage. Ma et al. [16] presented comprehensive research on the effects of process parameters, including lubrication, discharge voltage, and the blankholder force, on sheet deformation behavior.

The deformation velocity of the workpiece can reach hundreds of meters per second in less than 1 ms during the electromagnetic sheet metal forming process, which means the effect of air resistance on sheet deformation is non-negligible. Moreover, the air in the die cavity will be compressed with workpiece deformation, which leads to a sharp increase in air resistance and severe wrinkling of the deformed workpiece, as shown in Fig. 1.

However, the effect of air on electromagnetic sheet metal forming has not been comprehensively investigated. Recently, Cui et al. [17] found that, with a discharge voltage of 2 kV, while the surface quality of a workpiece with a vent hole is improved over a workpiece without a vent hole, the forming surface will still be concave. Moreover, this deformation is achieved only under a small coil with a small discharge voltage, and it is reasonable to believe that this phenomenon will become more obvious when the amount of deformation and discharge energy increase. Thus, in our team, to avoid the influence of the significant air resistance caused by high-speed deformation of the workpiece and the compression of the air in the die cavity, the cavity between the die and the workpiece is pumped into a near-vacuum environment whose pressure can be decreased to less than 100 Pa. Under near-vacuum conditions, Lai et al. [18] shaped a large sheet with a 1378 mm diameter of into an ellipsoid-shaped part via single discharge based on the advanced magnet technology and power supply system in the Wuhan High Magnetic Field Center.

Fig. 1 Photograph of deformed workpiece with wrinkling caused by air resistance

Actually, the effects of air on electromagnetic sheet metal forming can be summarized by the following three points when the die cavity is near vacuum: (1) the workpiece pre-deformation caused by atmospheric pressure when the die cavity is near vacuum; (2) the effect of workpiece pre-deformation on electromagnetic sheet metal forming; and (3) the effect of resistance caused by residual air in the die cavity on workpiece deformation. Accordingly, this paper presents a comprehensive investigation to determine the effects of air, such as workpiece pre-deformation caused by atmospheric pressure and air resistance generated by residual air in the die cavity, on sheet deformation behavior and the fitness between the die and workpiece through a combination of simulation and experimentation. The effects of workpiece thickness, material type and the die caliber on the pre-deformation are also analyzed.

2 Experiment

This section introduces the experimental design and procedure for workpiece deformation caused by atmospheric pressure when the die cavity is near vacuum. The experiments are conducted with sheets of varying thickness and materials under various die calibers to find the deformation law of the workpiece. Experiments used to investigate the effect of resistance generated by residual air in the die cavity on workpiece deformation are also designed and conducted.

2.1 Determination of sheet pre-deformation

2.1.1 Experimental design

Figure 2 shows the experimental setup sued to determine workpiece deformation caused by atmospheric pressure. In the experiments, the blank-holder force is loaded by a 1-ton clump weight. Moreover, a vacuum pump (shown in Fig. 2(d)) is used to extract the air in the die cavity between the workpiece and the die, and a vacuum gauge (shown in Fig. 2(c)) is used to detect the vacuum level of the die cavity. The dome depth is measured using a laser ranger to characterize workpiece deformation as shown in Fig. 2(a) and (b). The dome depths of the AA1060 materials with thicknesses of 1.5 mm, 2 mm, and 3 mm; AA2219 with thicknesses of 2.5 mm and 4 mm; and AA5083 with thicknesses of 1 mm, 1.5 mm, and 2 mm are measured.

The effects of the die caliber on workpiece pre-deformation are mainly investigated via simulation. The die is a semi-ellipsoid shape and the elliptic equation is described as:

$$\left(\frac{x}{m}\right)^2 + \left(\frac{y}{95}\right)^2 = 1 \tag{1}$$

where m is the long semi-axis, and the short semi-axis and die corner radius are constants equal to 95 mm and 20 mm, respectively. The caliber of the die varies with m, as shown in Fig. 3. The dome depths of workpieces with a thickness of 3 mm are calculated to reflect the deformation law of the workpiece. To investigate the adaptability of the deformation law to material type, the workpiece deformation with three types of materials (i.e., AA1060, AA2219, and AA5083) is calculated.

2.1.2 Experimental procedure

The measurement process consists of two steps:

Step 1: Measure the distance from the lower surface of the clump weight to the surface of the workpiece before the vacuum pump starts.
Step 2: Start the vacuum pump, observe the vacuum gauge number, and measure the distance from the lower surface of the clump weight to the surface of the workpiece again once the number stabilizes. Then, the dome depth of the workpiece can be obtained by calculating the difference between the two measurements.

2.2 Electromagnetic sheet metal forming

2.2.1 Experimental setup

Figure 4 shows the experimental setup, including a forming coil, a die, a workpiece, and a power supply system. The coil has one layer with 60-turn windings, an inner radius of 30 mm and an outer radius of 145 mm. The cross-sectional area of the copper wire is 1.5 mm × 16 mm and the inner-turn gap of the coil is 0.4 mm. High-strength material (Zylon fiber/epoxy

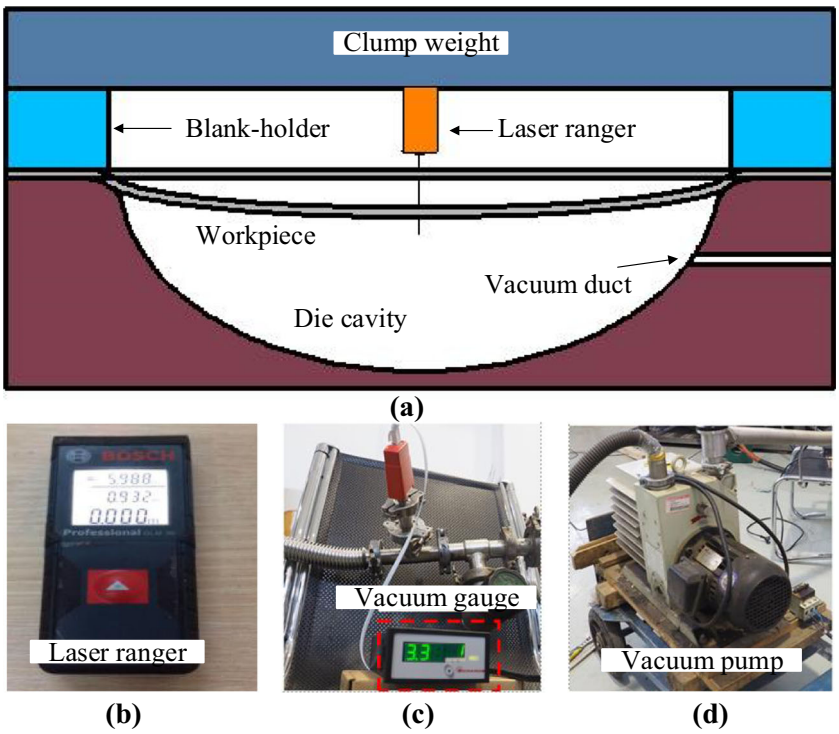

Fig. 2 Assembly drawing for measuring workpiece pre-deformation

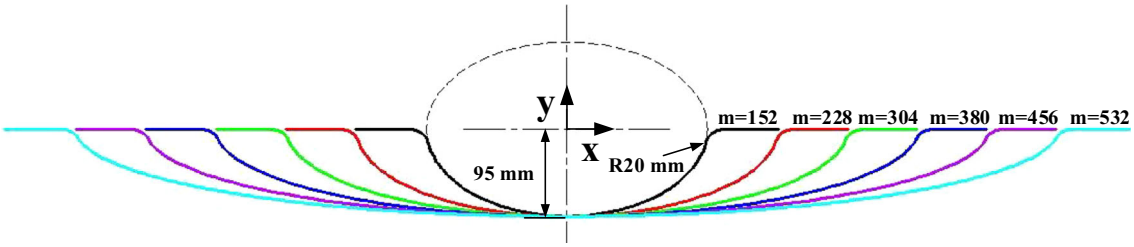

Fig. 3 Ellipsoidal dies with varied caliber

composite) is used to improve the structural strength. The generatrix of the inner surface of the die is a semi-ellipse with a major semi-axis of 152 mm and a minor semi-axis of 95 mm. The chamfer radius of the die mouth is 20 mm. A hole with a diameter of 8 mm is punched in sidewall of the die so to pump the air from the die cavity.

A circular workpiece with a thickness of 3 mm and a diameter of 398 mm is formed. The material of the workpiece is AA1060-O aluminum. The air pressure inside die cavity measured by vacuum gauge is used to characterize the amount of residual air. Low pressure means less residual air. Preliminary tests show that the air pressure inside the cavity can be reduced from 0.1 MPa to 30 Pa. The power supply system consists of two capacitors; each is 160 μF with a discharge range of 0–25 kV.

2.2.2 Experimental design and measurement

According to preliminary experimental results, the workpiece center contacts the die bottom when the discharge voltage is 10 kV. Therefore, to achieve a better die fitness for the deformed workpiece, the discharge voltage is determined to be 12.5 kV. Four levels of air pressure are set to produce different levels of air resistance, as shown in Table 1.

In this paper, the draw-in is defined as the reduction of the deformed workpiece radius. Here, the workpiece radius is the average of four radii evenly distributed along the circumferential direction. A 3D scanner is used to obtain the final forming shape of the workpiece and compare it with the die dimension to evaluate the effect of air resistance generated by various air pressures on the deformed workpiece profile.

3 Numerical model

This section introduces the numerical model, which includes the following: (1) the pre-deformation model of the workpiece when atmospheric pressure is used as the loading condition. This model can be used to predict workpiece pre-deformation caused by atmospheric pressure when the die cavity is a

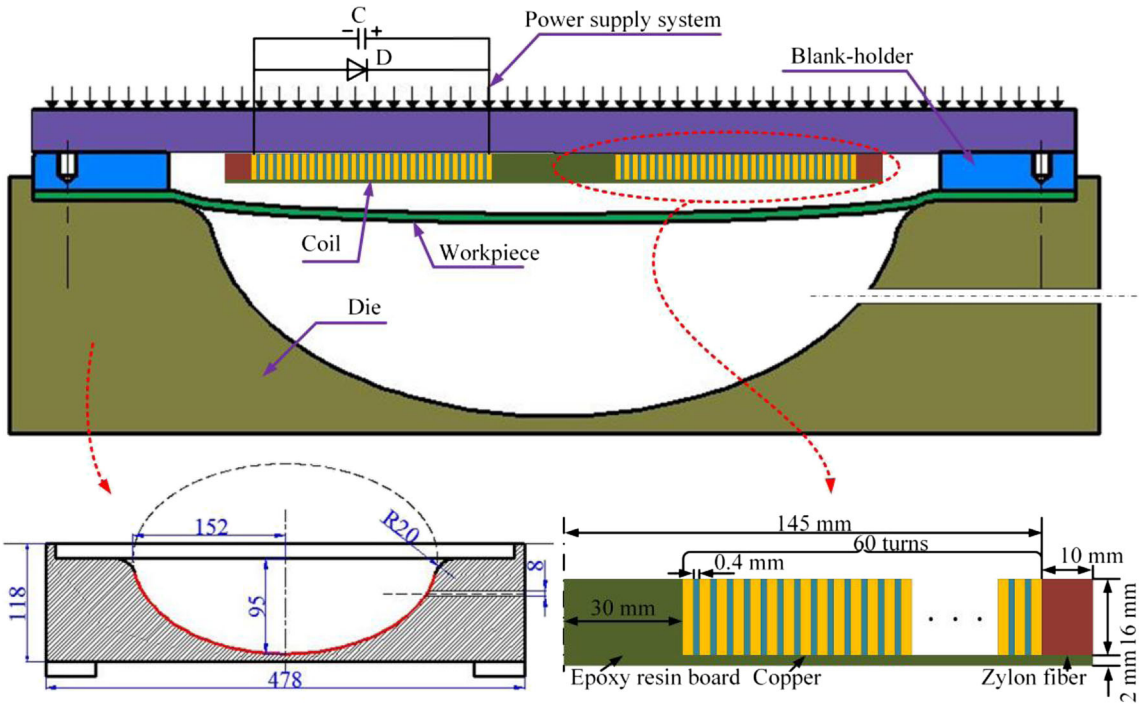

Fig. 4 Assembly of the electromagnetic forming system and detailed structures of the forming tools

Table 1 Parameters of sheet forming under various air pressures

Experiment	Discharge voltage	Air pressure
Exp. 1	12.5 kV	700 Pa
Exp. 2	12.5 kV	250 Pa
Exp. 3	12.5 kV	70 Pa
Exp. 4	12.5 kV	30 Pa

vacuum. (2) A model of electromagnetic sheet metal forming in terms of workpiece pre-deformation is devised. The distribution of electromagnetic force and workpiece deformation behavior of this model are compared with those of the traditional model.

3.1 Pre-deformation model

To avoid the influence of air resistance on workpiece deformation, the space between the die and the workpiece is brought to vacuum and remains under vacuum until the end of the discharge. However, the difference in air pressure between the outside and the die cavity increases with the decrease of die cavity pressure, which leads to workpiece pre-deformation before electromagnetic forming. To obtain the pre-deformed workpiece and investigate the effects of several parameters on pre-deformation, this section establishes the workpiece pre-deformation model when atmospheric pressure is used as the loading condition, as shown in Fig. 5.

To simplify the model and save calculation time, it is assumed that the loading of atmospheric pressure is positively correlated with time, and the time for loading pressure to rise from 0 to 1 atm is defined as 5 ms. Then, the atmospheric pressure remains constant for 5 ms to ensure stability of the sheet deformation, as shown in Fig. 6.

3.2 Electromagnetic-mechanical coupled model

To better understand the effect of pre-deformation on electromagnetic sheet metal forming, a coupled electromagnetic-mechanical numerical model was established based on the 2D axisymmetric solver in LS-DYNA. In this paper, to save calculation time, a 1/32 model is adopted.

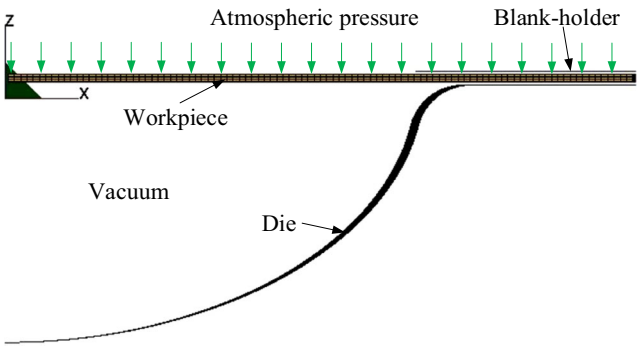

Fig. 5 Pre-deformation model when the die cavity is a vacuum

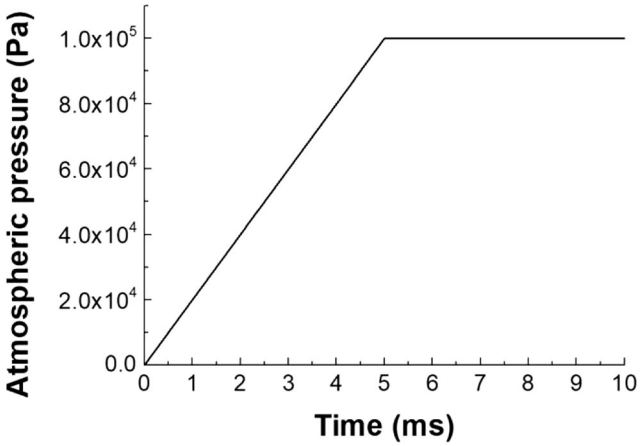

Fig. 6 The relationship of atmospheric pressure with time

3.2.1 Flowchart of the simulation model

Figure 7 shows the flowchart of the coupled electromagnetic-mechanical model. The sequential coupling method is applied to the electromagnetic model calculation when considering the effect of workpiece deformation, which significantly improves the accuracy, especially for the deformation of large workpieces.

The Lorentz force acting on the workpiece is calculated in the electromagnetic model, and then imported into the mechanical model to calculate the workpiece deformation. The new workpiece geometric information is fed back into the electromagnetic model and identified by updating the boundary element matrix. Based on the new workpiece geometry, the Lorentz force is calculated and imported into the mechanical model again to calculate the workpiece deformation in the next step. In this way, coupling of the two fields is achieved.

3.2.2 Electromagnetic model

The LS-DYNA electromagnetic module is realized by coupling finite element methods (FEM) for the solid conductors with boundary element methods (BEM) for the surrounding air. By using BEM, the model does not require air meshes, which is of great significance for electromagnetic forming. This method can both save the time required by traditional numerical EMF models to calculate air meshes (wherein air meshes should be constantly updated with the workpiece deformation) [20] and effectively avoid the problem of the model not converging due to air mesh distortion for some situations when workpiece deformation is severe or a higher speed impact exists between the die and the workpiece.

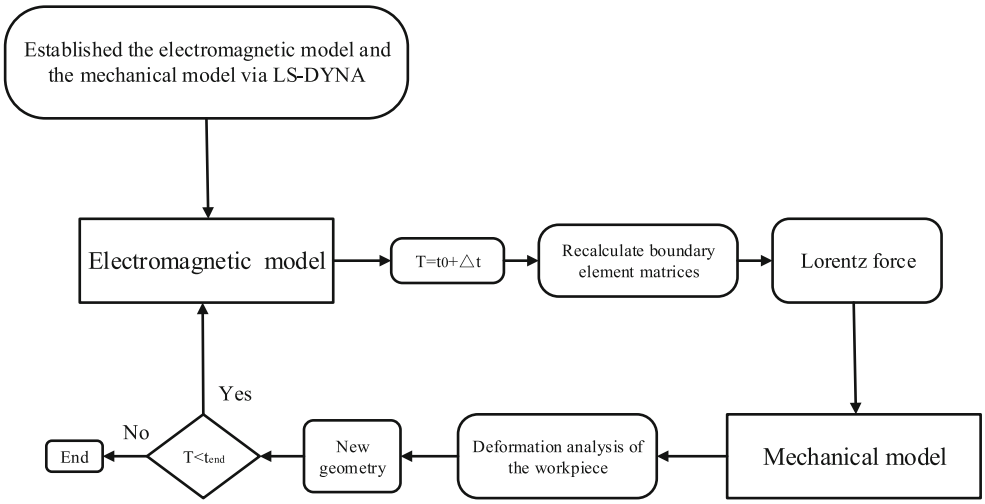

Fig. 7 Flowchart of the electromagnetic-mechanical coupling model

Because LS-DYNA is primarily a three-dimensional (3D) code, wherein most features are available only in 3D, 2D electromagnetic fields (2D-EMs) and 3D mechanical fields are coupled by the following methods [21]: First, a plane where 2D-EMs are calculated should be defined for each conducting part with a 3D mesh. Then, the solved EM fields are reported over the full 3D mesh by rotations around the axis. The initial discharge voltage is used as excitation to solve the coupled model. The line parameters, such as line capacitor, line inductor, line resistance, and initial discharge voltage, are set to be evenly spread between the various 2D circuits, as expressed in the following formulas:

$$R_i = \frac{R}{N}, L_i = \frac{L}{N}, C_i = NC, V_{0i} = \frac{V_0}{N} \tag{2}$$

where R_i, L_i, C_i and V_{0i} are resistance, inductance, capacitance, and discharge voltage of each circuit, respectively, and N is the total turns of the coil. The detailed circuit parameters of the forming system and the electromagnetic parameters of the materials are presented in Tables 2 and 3, respectively.

3.2.3 Mechanical model

The blank-holder is modeled using shell elements and is treated as a rigid body to increase calculation speed. To consider the effect of die deformation on workpiece deformation behavior during the impact between the die and the workpiece, the die is modeled using solid elements as an elastic body. Surface-to-surface contacts are defined between the workpiece and forming tools, where the workpiece is defined as the master surface and the die and blank-holder are defined as slave surfaces. The friction coefficient is set to 0.15. The workpiece is assumed to be an isotropic plasticity body and material properties are obtained through tensile tests at room temperature. The plots of measured and fitted stress against strain for three materials are shown in Fig. 8.

To consider the effect of strain rate on the workpiece flow stress, viscoplastic material behavior is assumed and the Cowper-Symonds constitutive model is used, as described by:

$$\sigma = \sigma_{qs}\left[1 + \left(\frac{\varepsilon_p^{\bullet}}{P}\right)^m\right] \tag{3}$$

where $\varepsilon^{\bullet}$ is the strain rate, and m and P are the constants of the aluminum alloy with values of 0.25 and 6500, respectively [20]. The detailed mechanical parameters of the material are presented in Table 4.

Table 2 Circuit parameters

Parameters	Description	Value
C	Line capacitor	320 μF
L	Line inductor	7 μH
R	Line resistance	25 mΩ
R_d	Crowbar resistance	300 mΩ

Table 3 Electromagnetic parameters of materials

Material types	Resistivity (γ)	Permeability (μ)
Workpiece		
AA1060	2.81e−8 Ω·m	$4\pi \times 10^{-7}$ H/m
AA2219	4.15e−8 Ω·m	$4\pi \times 10^{-7}$ H/m
AA5083	6.08e−8 Ω·m	$4\pi \times 10^{-7}$ H/m
Coil		
Copper	1.72e−8 Ω·m	$4\pi \times 10^{-7}$ H/m

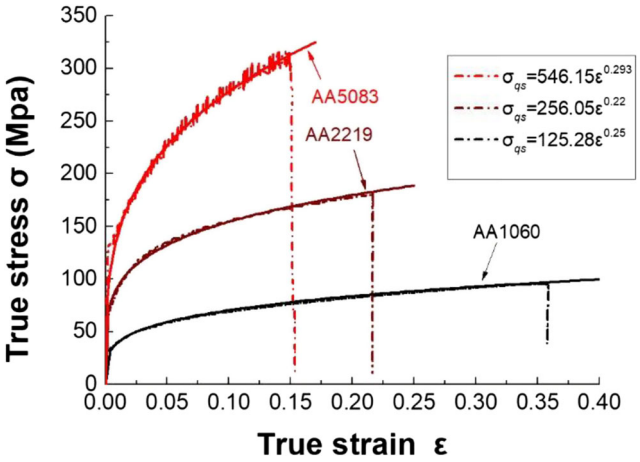

Fig. 8 True stress-strain curve of three materials under the quasi-static condition

4 Results and discussion

4.1 Parameters affecting workpiece pre-deformation

Figure 9 presents the calculated profile of the 3-mm-thick deformed AA1060 workpiece as a function of time. The axial deformation increases with time and reaches a maximum at approximately 7 ms, and then remains constant. The magnitude of the axial displacement at the center is larger than at other regions of the workpiece, and the maximum value is 11 mm.

4.1.1 Effects of thickness and material type of the workpiece

Figure 10 shows the effects of different thicknesses and material types on the workpiece pre-deformation. For the workpiece made of AA1060, the axial deformation increases as thickness decreases, as shown in Fig. 10(a). Moreover, the thinner the workpiece, the larger the increment of deformation. Figure 10(b) presents the workpiece deformation of three types of materials with a thickness of 2 mm. Their properties have been introduced in Section 3.2.3. It can be seen that the deformation decreases with the increase of material strength from AA1060 to AA5083. However, the deformation increment from AA2219 to AA5083 is much smaller than that from AA1060 to AA2219. This is because most of the deformation is still in the elastic stage for AA2219 and AA5083 due to their high yield strength. Furthermore, the dome depth of the workpiece calculated by the simulation model is compared with that measured by experiments, as shown in Fig. 10 (c). The results show a good agreement within a certain range of errors, which confirms the reliability of the model established in Section 3.1.

4.1.2 Effects of die caliber

The plot of calculated dome depth against die caliber shown in Fig. 11 presents their relationship for three materials. As die caliber increases, the dome depth of the workpiece increases and exhibits a near-liner relationship for AA1060 when the die caliber is larger than 450 mm. As die caliber increases, a near-liner relationship between the dome depth and die caliber occurs for AA2219 and AA5083. Furthermore, the difference of the dome depth for the three materials increases with the increase of die caliber, indicating that dome depth is more sensitive to material type as die caliber increases.

Figure 12 illustrates the draw-in of the pre-deformed workpiece with several materials. It can be seen that, when die caliber is less than 450 mm, the draw-in is less than 1 mm, and when die caliber is greater than 450 mm, the draw-in increases rapidly with die caliber increase. This phenomenon indicates that the draw-in caused by pre-deformation of the workpiece can be ignored when forming a workpiece into a die whose caliber is less than 450 mm. However, the effect of the draw-in on workpiece pre-deformation must be considered when forming large-scale parts that usually have diameters greater than 1000 mm because too much draw-in can lead to wrinkling of the pre-deformed workpiece.

Figure 13 shows the workpiece pre-deformation of AA1060. There are obvious wrinkles occurring on the workpiece near the chamfer of the die. Therefore, when forming a large-scale part, a larger initial blank-holder force should be applied to restrain the wrinkling failure of the pre-deformed workpiece.

Table 4 Mechanical parameters

Material types	Density (γ)	Yield stress	Young modulus (μ)	Poisson ratio
Workpiece				
AA1060	2713 kg/m^3	27.6 MPa	68.9 GPa	0.33
AA2219	2823 kg/m^3	75.8 MPa	73.1 GPa	0.33
AA5083	2657 kg/m^3	135 MPa	71.0 GPa	0.33
Coil				
Copper	8900 kg/m^3	–	110 GPa	0.34
Die				
Steel	7890 kg/m^3	–	200 GPa	0.33

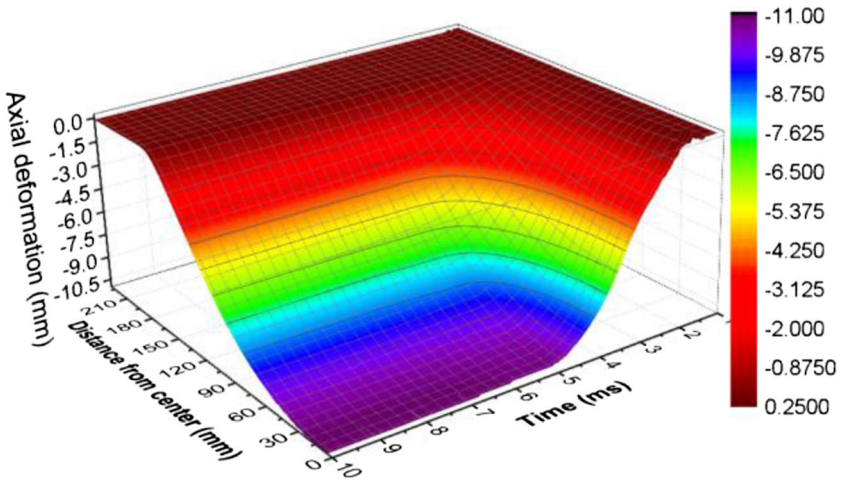

Fig. 9 Variation of sheet pre-deformation with time under the atmospheric pressure

4.2 Effect of pre-deformation on electromagnetic forming

The gap between coil and workpiece is one of the most important parameters for electromagnetic sheet metal forming, as it affects the coupling efficiency between the coil and the workpiece by affecting the magnetic field attenuation with distance. This phenomenon can be reflected by the current of the forming coil, as shown in Fig. 14. Two simulated currents with different simulation conditions are compared to the current measured in the EMF experiment.

Sim_1: Simulation considering the pre-deformation of the workpiece.
Sim_2: Simulation without considering the pre-deformation of the workpiece.
Exp.: Experiment in which the die cavity between the workpiece and the die is near vacuum.

Note that the drop edge of the measured current is in a state of continuous attenuation rather than oscillation attenuation as simulated. This is because a new discharge circuit

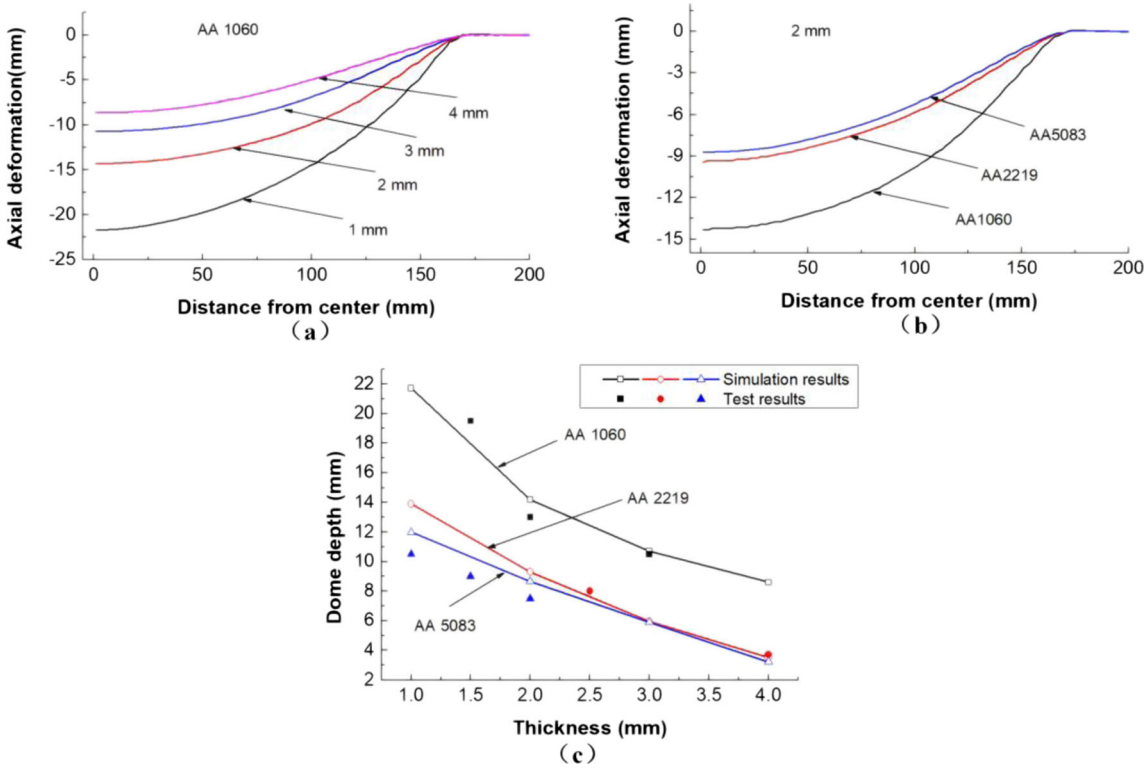

Fig. 10 Pre-deformation of the workpiece with different thicknesses and materials: (a) effect of thickness on sheet profiles, (b) effect of material types on sheet profiles, (c) effect of thickness and material types on dome depth of the workpiece

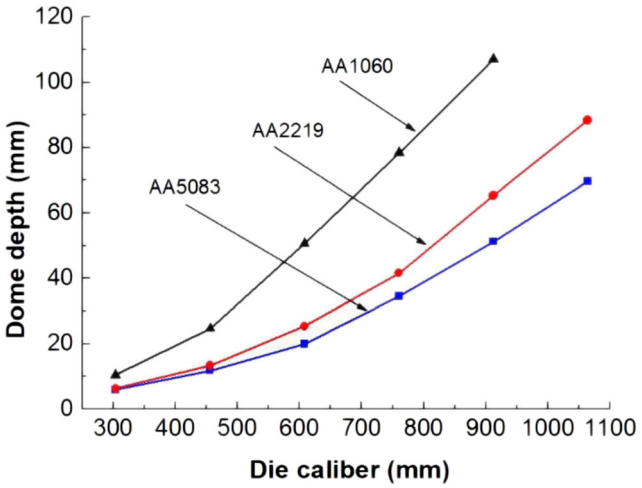

Fig. 11 Dome depth of the pre-deformed workpiece for several materials versus die caliber

configuration with a crowbar circuit is used in the experiments to reduce the heating and temperature rise of the forming coil, and thus prolong the service life of the forming coil without affecting the sheet deformation according to the investigation of Cao et al. [19]. It can be seen that the current of Sim_1 has a larger deviation (both in amplitude and time) than the current of Sim_2 when it reaches the peak value, whereas the current of Sim_1 is in good agreement with the current measure in the experiment. Based on the investigation of Cao et al., the period of the current can be simply calculated as $\frac{1}{4T_1}$, where T_1 means the time when the current reaches peak value at the first pulse. The time when the currents reaches peak value of the Sim_1 and the experiment are in good agreement as shown in Fig. 14, which indicates the periods of the two currents are the same. Therefore, the simulation considering the pre-deformation of the workpiece has high calculation accuracy.

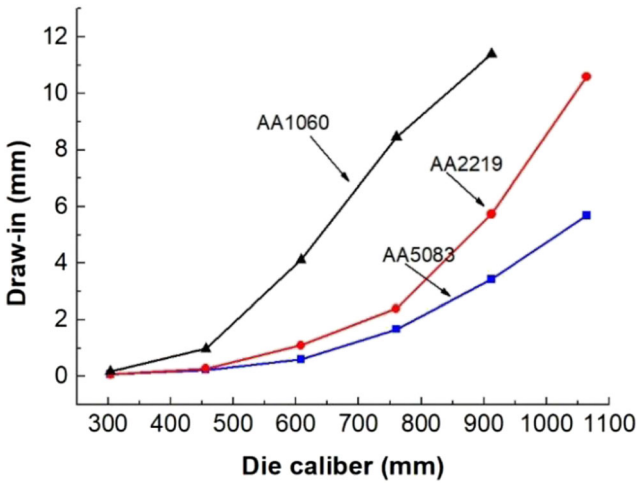

Fig. 12 Draw-in of the pre-deformed workpiece for several materials versus die caliber

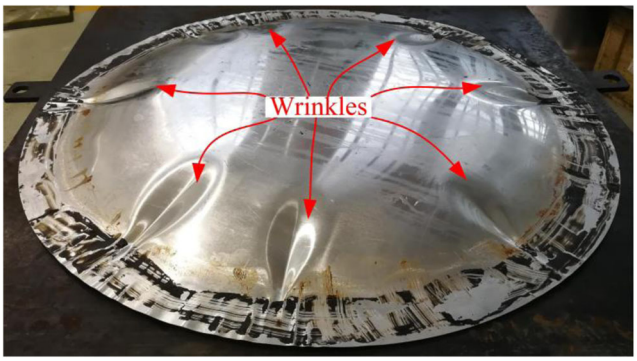

Fig. 13 Wrinkles of the pre-deformed workpiece

4.2.1 Distribution of electromagnetic force

Figure 15 compares the distribution of the Lorentz force acting on the workpiece at the initial forming stage of Sim_1 and Sim_2, as shown in Fig. 15(a) and (b), respectively. The time of the initial forming stage is determined as 100 μs because the workpiece is barely deformed at this time, which excludes the influence of deformation caused by EMF on the Lorentz force distribution. It can be seen that, when considering the pre-deformation of the workpiece in Sim_1, both the magnitude and distribution of the Lorentz force are obviously different from those of Sim_2. The Lorentz force is mainly concentrated on the deformation zone below the coil and reaches the peak value at the central area along the coil width when workpiece pre-deformation is not considered in Sim_2. Correspondingly, the position of the maximum Lorentz force moves toward the chamfer of the die because pre-deformation increases the gap between the coil and the workpiece, and the gap decreases gradually along the radial direction of the workpiece from the center to the outside.

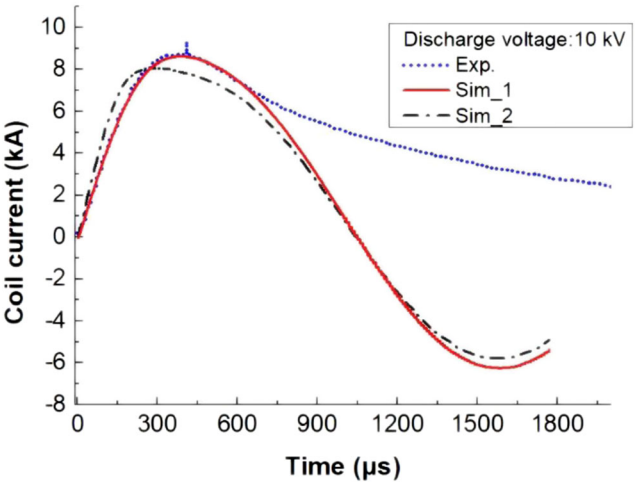

Fig. 14 Comparison of measured and calculated currents at a discharge voltage of 10 kV

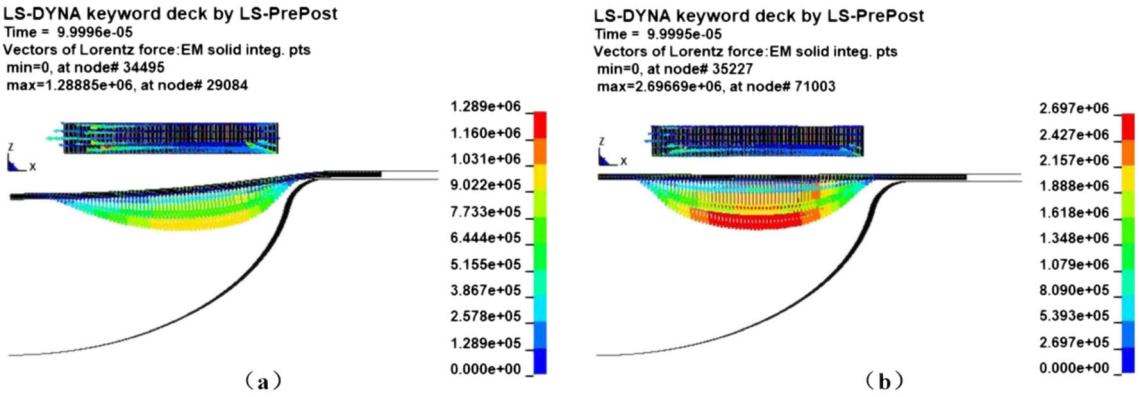

Fig. 15 Distribution of Lorentz force at 100 μs: (a) Sim_1 (b) Sim_2

The magnitude of the axial Lorentz force on the surface of the workpiece of Sim_2 is approximately 2.5 times larger than that of Sim_1 at 100 μs; however, the maximum Lorentz force is almost the same at 500 μs, indicating that the Lorentz force at the initial time plays a major role in electromagnetic sheet forming, as shown in Fig. 16.

4.2.2 Deformation velocity and sheet profile

The Lorentz force is the driving force for sheet deformation in the electromagnetic sheet metal forming process. Therefore, the magnitude and distribution of the Lorentz force will inevitably affect sheet deformation behavior. The axial velocity of the central workpiece produced by the inertia effect is one of the most important parameters for characterizing workpiece deformation behavior because inertia plays an important role in electromagnetic sheet metal forming according to the investigation of Kleiner et al. [10]. As shown in Fig. 17, the peak value of axial velocity at the center of the workpiece is reduced by 26.9% from 201 m/s to 147 m/s and the corresponding time is increased by 105 μs when pre-deformation is considered. In addition, the workpiece center velocity is negative at 960 μs in Sim_2, thus indicating that the workpiece center has collided with the bottom of the die and rebounded.

Figure 18 presents a comparison of deformed workpiece draw-in under two simulated conditions and an experiment. The result of Sim_1 shows better agreement with the experimental result, and the deviation is less than 0.4%. The draw-in of Sim_2 is 28.1 mm, and the deviation is more than 16.6%, thus indicating that the accuracy of models that consider workpiece pre-deformation is higher than those that do not consider pre-deformation.

Figure 19 compares the final profiles of the deformed workpiece obtained via both experimentation and simulation. The results of Sim_1 match the experiment well considering that the pre-deformation is caused by atmospheric pressure. These results can be predicted on the basis of the above analysis of the electromagnetic distribution and draw-in of the deformed workpiece. In Fig. 19, the axial deformation of Sim_1 is almost consistent with that of the experiment. For the result of Sim_2, the workpiece dome area impacts the die bottom and rebounds due to its higher velocity, thus indicating that the model that does not consider pre-deformation overestimates the profile of the workpiece. Therefore, the subsequent

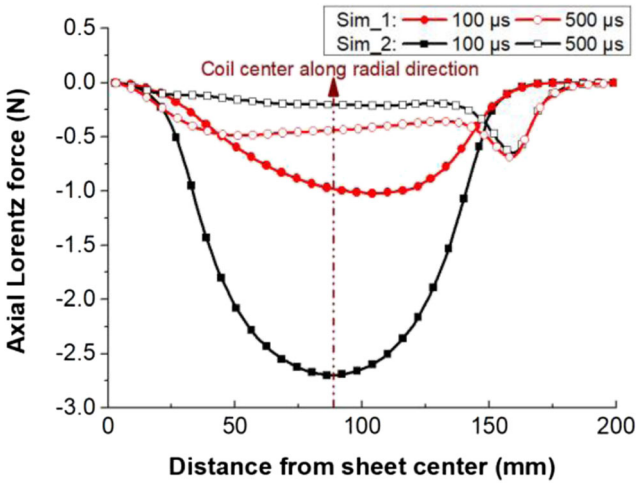

Fig. 16 Axial Lorentz force on the surface of the workpiece

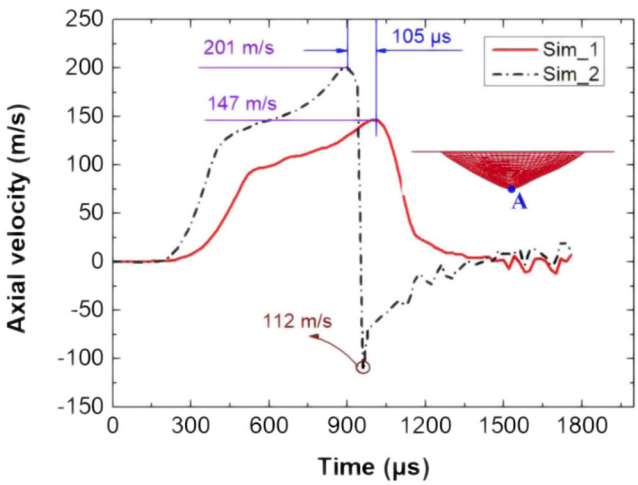

Fig. 17 Axial velocity of the workpiece center

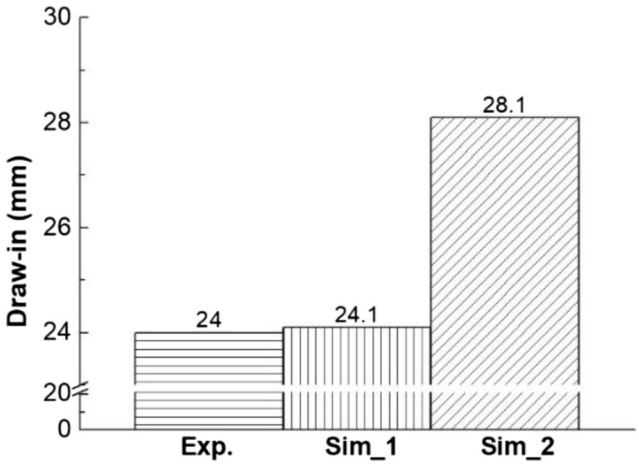

Fig. 18 Draw-in of the deformed workpiece

simulation calculations in this paper have considered the workpiece pre-deformation caused by atmospheric pressure.

4.3 Effect of air resistance in die cavity on electromagnetic forming

The aim of this section is to investigate the effect of resistance generated by residual air on workpiece deformation when the die cavity is near vacuum through the control of air pressure.

4.3.1 Profile of deformed workpiece

Figure 20 shows the final profiles of the deformed workpiece when the discharge voltage is 12.5 kV and the die cavity air pressure is 700 Pa, 250 Pa, 70 Pa, and 30 Pa. It can be seen that, when the air pressure in the die cavity is 700 Pa, obvious wrinkling occurs in the dome area of the workpiece and circumferential wrinkling occurs in the region not far from the dome area, as shown in Fig. 20(a). This phenomenon can be explained by combining the workpiece deformation process in ideal vacuum, as shown in Fig. 21. Three typical regions are divided along the radial direction of the deformed workpiece. Region A is the rebound area after the workpiece collides with the die. Region B represents the area on the workpiece that does not collide with the die. Region C is defined as the area

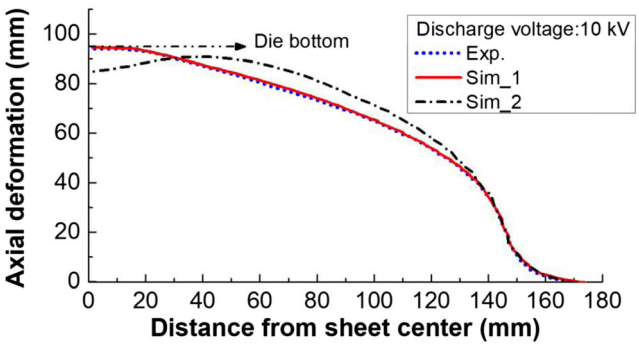

Fig. 19 Workpiece profiles in a 10-kV discharge voltage

where the deformed workpiece has better fit with the inner surface of the die.

In Fig. 21(a), the workpiece has not collided with the die yet; however, according to the trend, the center of the workpiece first collides with the bottom of the die due to the inertia caused by the uneven distribution of the Lorentz force, and then, the workpiece center rebounds after impacting with the die and region B near the workpiece center continues to deform toward the die, as shown from Fig. 21(b)–(d). In this process, the residual air in the die cavity is compressed at high speed into the space between the workpiece and the die in region B. Additionally, the air compressed at a high speed generates significant resistance, which leads to circumferential wrinkling. In addition, there is no extra place to drain the residual air, which results in a pit near the center of the workpiece. The results indicate that, when the air pressure in the die cavity is 700 Pa, there is still too much residual air generating large resistance and causing workpiece wrinkling. When the air pressure is reduced to 250 Pa, although both the circumferential wrinkling and the pit still occur on the workpiece, the degree of wrinkling is significantly reduced, as shown in Fig. 20(b). When the air pressure is reduced to 70 Pa, the circumferential wrinkling has disappeared and only a little pit occurs in the workpiece center, as shown in Fig. 20(c). Further, when the air pressure is reduced to 30 Pa, no wrinkling occurs on the whole workpiece, as shown in Fig. 20(d). Here, it should be noted that the minimum air pressure in the die cavity is 30 Pa due to the sealing limitation of the equipment. Therefore, workpiece deformation below 30 Pa can be obtained only by simulation of ideal vacuum.

According to Fig. 20(a)–(d), too much residual air in the die cavity is unfavorable to workpiece deformation because it will be compressed at high speed with large resistance, which leads to wrinkling. According to Figs. 20(d) and 21(d), when the air pressure is 30 Pa, the wrinkling caused by air resistance is effectively avoided. Moreover, compared with the simulation results, the rebound of the center caused by the collision between the workpiece and the die bottom is restrained in the experiments. The exact cause of this phenomenon cannot be determined due to the interaction between the die and the sheet is a transient and complex process. The possible reason may be that the constitutive model of the sheet material has changed under high-speed impact, and the model used in this paper is not suitable for impact analysis.

4.3.2 Die fitness of deformed workpiece

To evaluate the dimensional accuracy of the deformed parts shown in Fig. 22(a)–(d) at several air pressures in the die cavity, 3D measuring technology is used to obtain the workpiece profile with a 3D scanner, as shown in Fig. 22(e). Then, the workpiece profile is compared with the die established by Solidworks software according to the designed dimensions, as

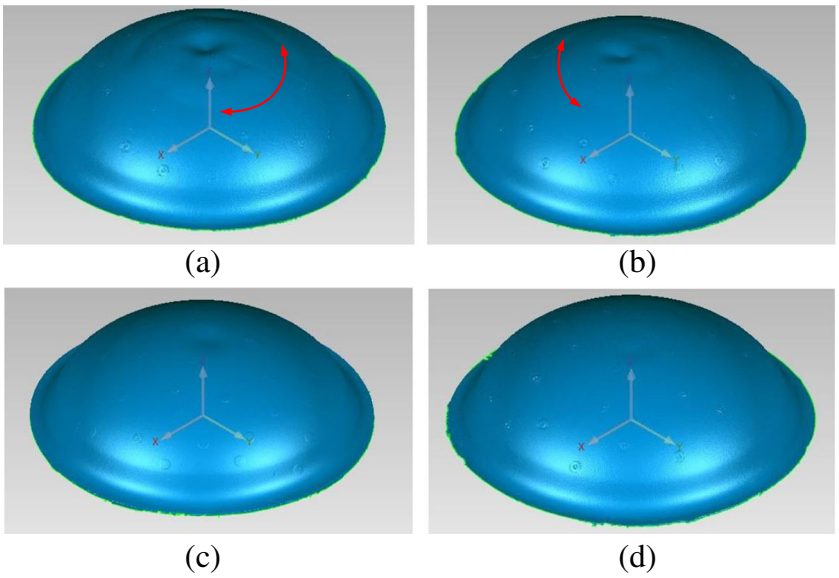

Fig. 20 Workpiece profiles for several air pressures in the die cavity: (a) 700 Pa (b) 250 Pa, (c) 70 Pa, and (d) 30 Pa

shown in Fig. 22(f). Finally, the workpiece is cut longitudinally along the path that passes through the center to obtain the contour lines of the workpiece and the die, as shown in Fig. 22(g).

Fig. 23 shows the contour lines of the vertical cross-section of the workpiece and die. The rebound height decreases with air pressure. When air pressure decreases to 30 Pa from 700 Pa, the rebound height is reduced by 75.9% from 5.111 mm to 1.232 mm, which is less than 1.5% of the die depth, thus indicating that the residual air has an obvious influence on workpiece rebound. In addition, most of the deformed workpiece has a good fit with the inner surface of the die. The relatively large gaps are mainly distributed in two regions: (1) region C near bottom of the die, as shown in Fig. 23(d) by the green circle; and (2) regions A and B near the die chamfer, as shown in Fig. 23(d) by the red circle. The gaps at regions A and B are 0.6033 mm and 0.7561 mm, respectively.

5 Conclusions

This paper comprehensively demonstrates the effects of air on electromagnetic sheet metal forming and includes the analysis of workpiece pre-deformation caused by atmospheric pressure when the cavity between the workpiece and the die is near the vacuum, the effect of sheet pre-deformation on

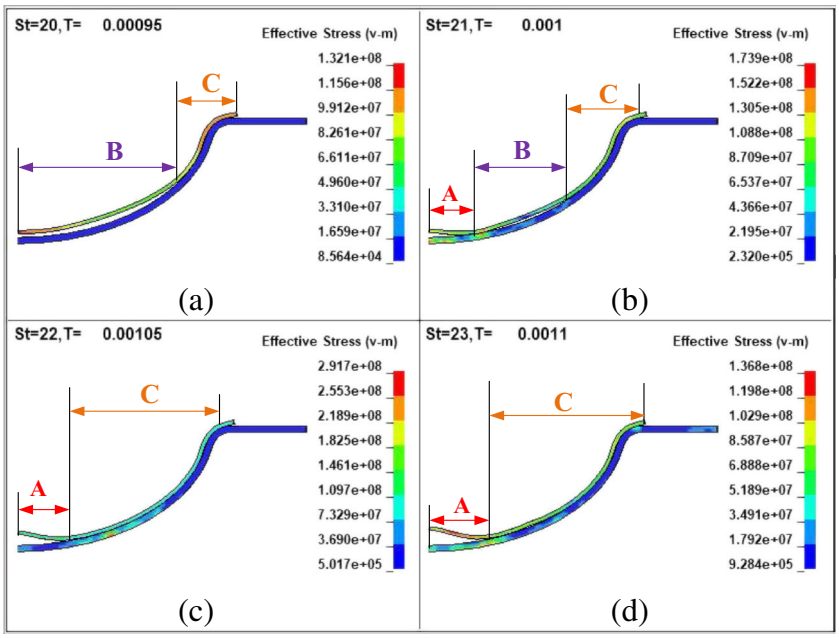

Fig. 21 Four stages of collision between workpiece and die: (a) 950 μs, (b) 1000 μs, (c) 1050 μs, and (d) 1100 μs

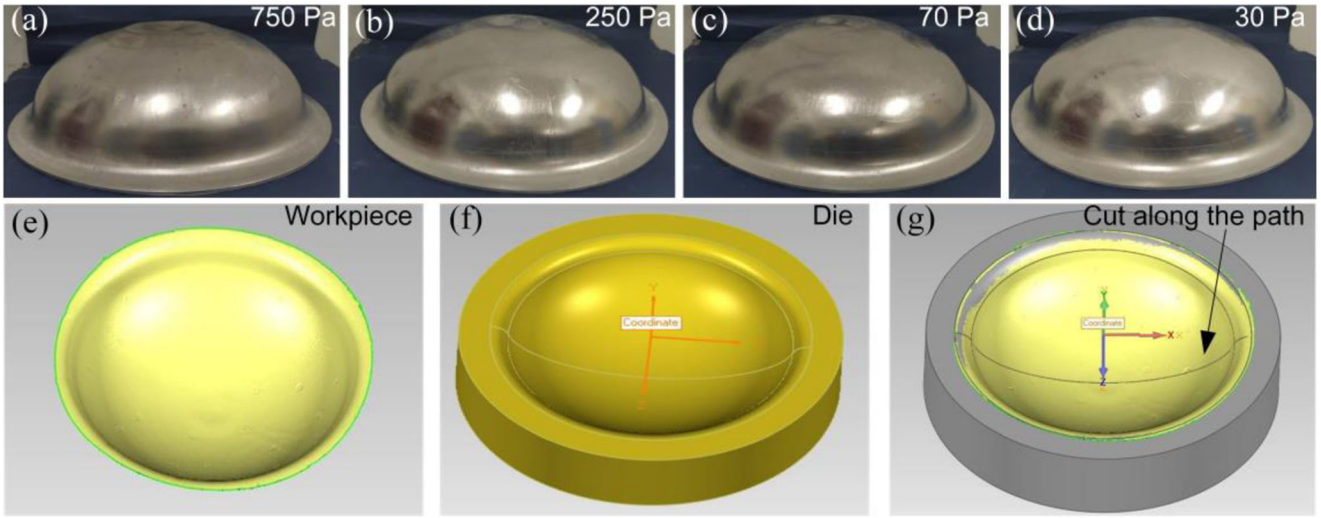

Fig. 22 Pictures of the deformed parts and their dimensional comparison with the die: (a)–(d) pictures of the deformed parts (e) scan data of workpiece, (f) the die built by Solidworks, (g) combination of workpiece and die

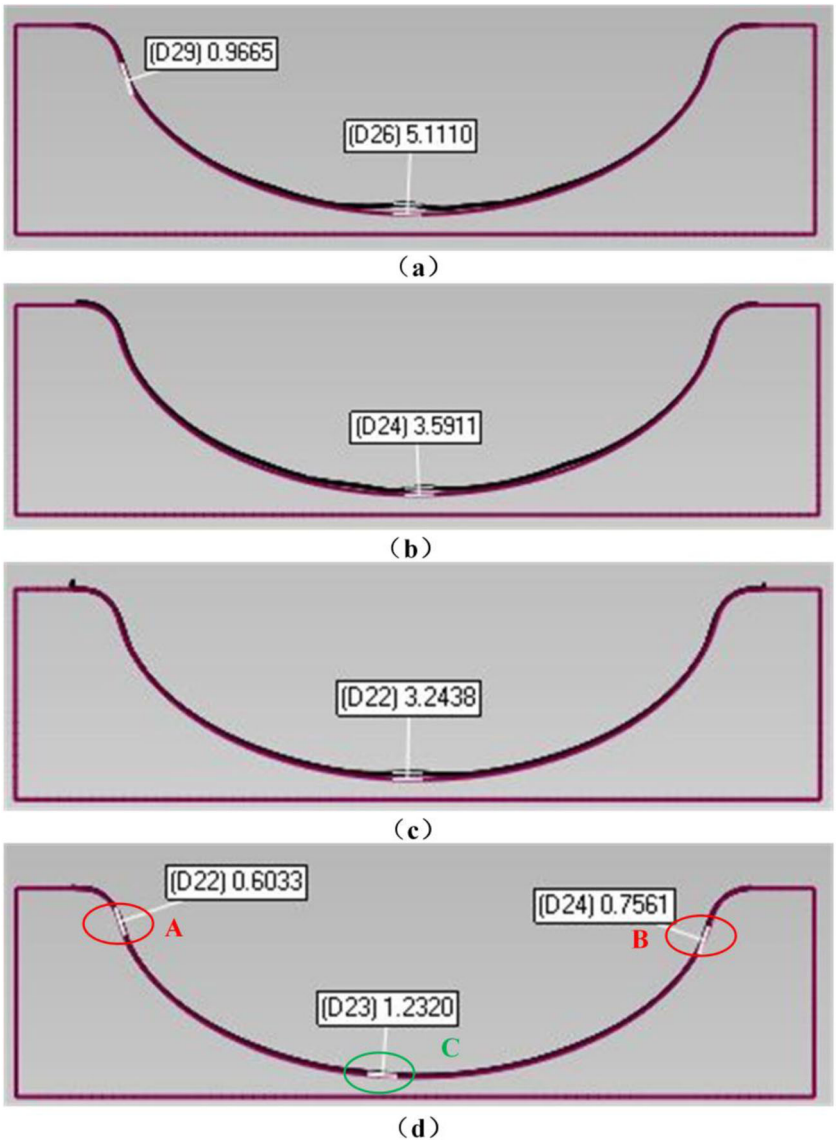

Fig. 23 Contour lines of the workpiece and die vertical cross-section for several air pressures: (a) 700 Pa, (b) 250 Pa, (c) 70 Pa, and (d) 30 Pa

electromagnetic forming, and the investigation of the effect of the air pressure in the die cavity on workpiece deformation. The following conclusions can be drawn:

1) Atmospheric pressure leads to workpiece pre-deformation when the die cavity is pumped to vacuum. Then, the pre-deformation of the workpiece will affect the EMF process. The results show that the magnitude of the Lorentz force acting on the workpiece and the deformation velocity of the workpiece center are reduced by 60% and 26.9%, respectively, due to workpiece pre-deformation when the discharge voltage is 10 kV. The distribution of the Lorentz force tends to move toward the region near the die chamfer. The model that considers workpiece pre-deformation provides a more accurate calculation of electromagnetic sheet metal forming than the model does not consider the workpiece pre-deformation.
2) Based on the simulation and experimental results, the resistance generated by residual air when the die cavity is near vacuum obviously affects workpiece deformation. Too large an air pressure in the die cavity will cause wrinkles in the workpiece. When the air pressure in the die cavity is reduced to 30 Pa, the maximum deviation of die fittability is less than 1.5%, which effectively ensures workpiece forming accuracy.

Funding information This work was supported by the National Basic Research Program of China (973 Program): Grant No. 2011CB012801, the National Key Research and Development Program of China (Grant No. 2016YFA0401701), and the China Postdoctoral Science Foundation: 2018M632856.

References

1. Psyk V, Risch D, Kinsey BL, Tekkaya AE, Kleiner M (2011) Electromagnetic forming-a review. J Mater Process Technol 211: 787–829. https://doi.org/10.1016/j.jmatprotec.2010.12.012
2. Correia JPM, Siddiqui MA, Ahzi S, Belouettar S, Davies R (2008) A simple model to simulate electromagnetic sheet free bulging process. Int J Mech Sci 50(10):1466–1475. https://doi.org/10.1016/j.ijmecsci.2008.08.008
3. Yu HP, Li CF (2009) Effects of current frequency on electromagnetic tube compression. J Mater Process Technol 209(2):1053–1059. https://doi.org/10.1016/j.jmatprotec.2008.03.011
4. Yu HP, Fan ZS, Li CF (2014) Magnetic pulse cladding of aluminum alloy on mild steel tube. J Mater Process Technol 214(2):141–150. https://doi.org/10.1016/j.jmatprotec.2013.08.013
5. Yu HP, Tong YC (2017) Magnetic pulse welding of aluminum to steel using uniform pressure electromagnetic actuator. Int J Adv Manuf Technol 91:2257–2265. https://doi.org/10.1007/s00170-016-9928-y
6. Takatsu N, Kato M, Sato K, Tobe T (1988) High-speed forming of metal sheets by electromagnetic force. JSME Int J 31(1):142–148. https://doi.org/10.1299/jsmec1988.31.142
7. Oliveira DA, Worswick MJ, Finn M, Newman D (2005) Electromagnetic forming of aluminum alloy sheet: free-form and cavity fill experiments and model. J Mater Process Technol 170(1): 350–362. https://doi.org/10.1016/j.jmatprotec.2005.04.118
8. Kamal M, Daehn GS (2007) A uniform pressure electromagnetic actuator for forming flat sheets. J Manuf Sci Eng 129(2):369–379. https://doi.org/10.1115/1.2515481
9. Ahmed M, Panthi SK, Ramakrishnan N, Jha AK, Yegneswaran AH, Dasgupta R, Ahmed S (2011) Alternative flat coil design for electromagnetic forming using FEM. Trans Nonferrous Metals Soc China 21(3):618–625. https://doi.org/10.1016/S1003-6326(11)60759-0
10. Kleiner M, Beerwald C, Homberg W (2005) Analysis of process parameters and forming mechanisms within the electromagnetic forming process. CIRP Ann Manuf Technol 54(1):225–228. https://doi.org/10.1016/S0007-8506(07)60089-4
11. Shang JH, Daehn GS (2011) Electromagnetically assisted sheet metal stamping. J Mater Process Technol 211(5):868–874. https://doi.org/10.1016/j.jmatprotec.2010.03.005
12. Cui XH, Mo JH, Li JJ, Xiao XT, Zhou B, Fang JX (2016) Large-scale sheet deformation process by electromagnetic incremental forming combined with stretch forming. J Mater Process Technol 237:139–154. https://doi.org/10.1016/j.jmatprotec.2016.06.004
13. Lai ZP, Cao QL, Zhang B, Han XT, Zhou ZY, Xiong Q, Zhang X, Chen Q, Li L (2015) Radial Lorentz force augmented deep drawing for large drawing ratio using a novel dual-coil electromagnetic forming system. J Mater Process Technol 222:13–20. https://doi.org/10.1016/j.jmatprotec.2015.02.029
14. Lai ZP, Cao QL, Han XT, Huang YJ, Deng FX, Chen Q, Li L (2017) Investigation on plastic deformation behavior of sheet workpiece during radial Lorentz force augmented deep drawing process. J Mater Process Technol 245:193–206. https://doi.org/10.1016/j.jmatprotec.2017.02.010
15. Cui XH, Li JJ, Mo JH, Fang JX, Zhou B, Xiao XT (2016) Effect of the sheet thickness and current damping exponent on the optimum current frequency in electromagnetic forming. Int J Adv Manuf Technol 85(1–4):843–851. https://doi.org/10.1007/s00170-015-7983-4
16. Ma HJ, Huang L, Li JJ, Duan XC, Ma F (2018) Effects of process parameters on electromagnetic sheet free forming of aluminum alloy. Int J Adv Manuf Technol 96(1–4):359–369. https://doi.org/10.1007/s00170-018-1589-6
17. Cui XH, Mo JH, Li JJ, Zhao J, Zhu Y, Huang L, Li ZW, Zhong K (2014) Electromagnetic incremental forming (EMIF): a novel aluminum alloy sheet and tube forming technology. J Mater Process Technol 214(2):409–427. https://doi.org/10.1016/j.jmatprotec.2013.05.024
18. Lai ZP, Cao QL, Han XT, Liu N, Chen M, Li XX, Huang YJ, Chen Q, Li L (2018) Application of electromagnetic forming as a light-weight manufacturing method for large-scale sheet metal parts. In: Proceedings of the 8th International Conference on High Speed Forming-ICHSF, Ohio, American. doi:https://doi.org/10.17877/DE290R-18984
19. Cao QL, Han XT, Lai ZP, Xiong Q, Zhang X, Chen Q, Xiao HX, Li L (2015) Analysis and reduction of coil temperature rise in electromagnetic forming. J Mater Process Technol 225:185–194. https://doi.org/10.1016/j.jmatprotec.2015.02.006
20. Yu HP, Li CF, Deng JH (2009) Sequential coupling simulation for electromagnetic-mechanical tube compression by finite element analysis. J Mater Process Technol 209(2):707–713. https://doi.org/10.1016/j.jmatprotec.2008.02.061
21. Pierre LE, Iñaki C (2015). Recent developments in the electromagnetic module: a new 2D axi-symmetric EM solver. https://www.dynalook.com/10th-european-ls-dyna-conference/11%20Developer%20III%20-%20Multiphysics/03-LEplattenier-LSTC-P.pdf